Research Article | Vol. 29, No. 14 / 5 July 2021 / Optics Express 21160
Optics EXPRESS

Enhancement of the indistinguishability of single photon emitters coupled to photonic waveguides

J. GUIMBAO,* L. M. WEITUSCHAT, J. M. LLORENS MONTOLIO, AND P. A. POSTIGO

Instituto de Micro y Nanotecnología, IMN-CNM, CSIC (CEI UAM+CSIC) Isaac Newton, 8, E-28760 Tres Cantos, Madrid, Spain
*j.guimbao@csic.es

Abstract: One of the main steps towards large-scale quantum photonics consists of the integration of single photon sources (SPS) with photonic integrated circuits (PICs). For that purpose, the PICs should offer an efficient light coupling and a high preservation of the indistinguishability of photons. Therefore, optimization of the indistinguishability through waveguide design is especially relevant. In this work we have developed an analytical model that uses the Green's Dyadic of a 3D unbounded rectangular waveguide to calculate the coupling and the indistinguishability of an ideal point-source quantum emitter coupled to a photonic waveguide depending on its orientation and position. The model has been numerically evaluated through finite-difference time-domain (FDTD) simulations showing consistent results. The maximum coupling is achieved when the emitter is embedded in the center of the waveguide but somewhat surprisingly the maximum indistinguishability appears when the emitter is placed at the edge of the waveguide where the electric field is stronger due to the surface discontinuity.

1. Introduction

Indistinguishability of single photons generated by point defects is the central topic of quantum photonic integrated circuits for quantum information applications like quantum simulation [1], quantum teleportation [2] or quantum networks [3]. Indistinguishable photons are usually generated by parametric down-conversion [4] or alternatively from a single two-level quantum emitter in a solid-state environment [5]. Over the last years several on-chip integration of different SPS material systems have been demonstrated: III-V quantum dots [6], carbon nanotubes [7], NV [8] or SiV centers in diamond [9] and 2D layered materials [10]. For most of those solid-state quantum emitters the intrinsic indistinguishability at room temperature is almost zero because pure dephasing rates are orders of magnitude larger than the population decay rate [11]. Improvement of the indistinguishability can be achieved by low temperature operation and by reducing the radiative lifetime of the SPS using an optical cavity that takes advantage of the Purcell effect [12]. The balance between dephasing and population decay rates varies significantly depending on the material system. Whereas for specific single self-assembled GaAs quantum dots the emission at low temperature can be radiative lifetime limited [13], defects in 2D materials can exhibit several orders of magnitude of difference between radiative decay and pure dephasing rates [14]. Purcell enhancement using photonic resonators permits on-chip control of light−matter interaction to enhance collection efficiency and generation of indistinguishable photons [15] that can be used for on-chip processing of quantum information [16–18]. Therefore, it is important to explore the coupling of SPS to PICs and its effect on the indistinguishability. In this work we use an analytical treatment of light radiation from a point source placed at an arbitrary location and with arbitrary orientation on a waveguide. The refractive indexes of the waveguide correspond to materials commonly used in silicon photonics (SiO_2, Si_3N_4, Si)

#422023 https://doi.org/10.1364/OE.422023
Journal © 2021 Received 10 Feb 2021; revised 14 May 2021; accepted 9 Jun 2021; published 22 Jun 2021

Optics EXPRESS

besides other high-index materials like WeS_2 or WO_3 [19]. It is worth to note that other specially designed nanomaterials with ultra high refractive index can be designed [20]. We explore how the position of the source and its orientation affects the coupling to the waveguide modes and the indistinguishability of the photons. We also explore how the dimensions of the waveguide impact the indistinguishability. We perform FDTD simulations to validate the analytical model and to calculate the Purcell effect. The results show remarkable differences depending on the orientation of the SPS and provide maximum indistinguishability when the source is placed at the edge of the waveguide, in contrast to the maximum coupling efficiency position at the center of the waveguide. The indistinguishability is expressed in terms of the pure dephasing value of the emitter, so that the effects of the waveguide can be compared between strong and weak dissipative emitters. Depending on the waveguide geometry and the position of the source the indistinguishability can either increase or decrease, showing non-negligible enhancements for weak dissipative emitters placed at optimum positions.

Several works deal with the radiation of a point source embedded in bounded dielectric slabs and square waveguides through Green's function methods [21–26]. Also, the problem of the unbounded dielectric slab is treated in [27] from a classical perspective and in [28] from a quantum perspective. However, in those cases the description of the source comes from the macroscopic expression of the dipole moment, without computing the Green's Dyadic. The Green's function of the unbounded 2D dielectric slab is covered in [29] and the same for the 3D cylindrical fiber in [30–32] through the development of a transform theory. As far as we know, the Green's Dyadic of a 3D unbounded rectangular waveguide has not been treated until this work. Here we develop a generalization of the transform theory from the 2D case [29] to obtain the solution of the 3D version of the problem for an unbounded rectangular waveguide. The obtention of the Green's Dyadic allows us to directly connect the value of the indistinguishability with the geometrical parameters of the waveguide, which also has not been covered neither in the previously mentioned works.

2. Methods, results and discussion

2.1. Indistinguishability for different SPS

In an isolated two-level system, the emission rate can be fully described by its population decay rate Γ_0. However, a solid-state quantum emitter has an interaction with the mesoscopic environment. The two-level system is affected by random fluctuations of its energy that can be described by a stationary stochastic process characterized by a dephasing rate Γ^* [33]. In this situation the indistinguishability (I) is reduced to [34]:

$$I = \frac{\Gamma_0}{\Gamma_0 + \Gamma^*}\ , \tag{1}$$

In general, for any practical implementation in quantum information processing $I \geq 0.5$ [33]. The pure dephasing rates at room temperature of solid-state quantum emitters like color centers, quantum dots or organic molecules are about 3 to 6 orders of magnitude larger than their radiative decay rates [34]. Improvement of this efficiency can be achieved by working at cryogenic temperatures. For example, for excitons weakly confined in GaAs quantum dots the dot ground-state transition at low temperature is near radiative life-time limited [13] which would provide a balance of about $\Gamma^*/\Gamma_0 \approx 1$ and I $\approx$ 0.5. There are recent reports of even better performance with strain free GaAs/AlGaAs quantum dots without the need of Purcell enhancement [35]. For those highly efficient emitters the ratio $\Gamma^*/\Gamma_0 \to 0$ and the intrinsic indistinguishability tends to the unity. As an example of an intermediate situation, InAs quantum dots have decay and pure dephasing rates $\Gamma^*/\Gamma_0 = 2.6$ [36,37] and the indistinguishability is only $I \approx 0.19$. On the opposite side, strain-induced defects in 2D materials have typical radiative lifetimes in the order of nanoseconds with dephasing lifetimes in the order of picoseconds [14]. For those emitters the

Optics EXPRESS

Γ^*/Γ_0 balance reaches 10^3 with almost zero indistinguishability. However, recent works related to defects created in transition metal dichalcogenides (like MoS_2) by local helium ion irradiation [38] show radiative lifetimes < 150 ps. Also, a lifetime < 100 ps has been observed recently in regular strain induced defects in WSe_2 layers deposited on metallic surfaces [39, 40]. More examples of quantum emission demonstrations in 2D materials can be found in [41]. Therefore, emitters with a certain Γ^*/Γ_0 ratio may enhance significantly their indistinguishability when properly integrated inside photonic waveguides due to the change in their radiative decay rate. We will show that for certain geometries and emitter positions I can be greatly reduced whereas optimal configurations can maintain or even enhance I significantly, especially for emitters with a certain Γ^*/Γ_0 ratio.

2.2. Analytic model for pure dephasing

We can assume that for a two-level emitter coupled to a waveguide the coupling (g) and the cavity decay rate (κ) are in the incoherent limit ($2g \ll \Gamma_0+\Gamma^*+\kappa$) and "bad cavity" regime ($\kappa \gg \Gamma_0+\Gamma^*$) [34]. In that limit the cavity can be adiabatically eliminated so the dynamics of the coupled system are described by an effective quantum emitter with decay rate ($\Gamma+R$) where R is the population transfer between the emitter and the cavity [34]:

$$I = \frac{(\Gamma_0 + R)}{(\Gamma_0 + R) + \Gamma^*} \; ; \; R = \frac{4g^2}{\Gamma_0 + \Gamma^* + \kappa} \quad , \tag{2}$$

R is related to the Purcell enhancement (P_f) by $R = \Gamma_0 \cdot P_f$ [42]. Substituting in Eq. (2) we obtain:

$$I = \frac{(1 + P_f)}{(1 + P_f) + \frac{\Gamma^*}{\Gamma_0}} \, , \tag{3}$$

here the Purcell enhancement is defined as Γ/Γ_0 where Γ is the population decay rate in the inhomogeneous environment. This ratio is related to the power emitted by the source [43]:

$$\frac{\Gamma}{\Gamma_0} = \frac{P}{P_0} \, , \tag{4}$$

with P and P_0 the power emitted in the inhomogeneous and homogeneous environment, respectively. The radiative decay rate enhancement can be obtained by FDTD simulations integrating the power emitted by the source inside the waveguide (P) and normalizing it with respect to the power in a homogeneous surrounding (P_0). In order to extract the maximum amount of physical information from the interaction between the quantum emitter and the photonic waveguide, we develop an analytic model of the system. We use the relation between Γ and the Green dyadic of the equation governing the interaction between the source and the waveguide. From Eq. (4) one can obtain the dependence of the decay rate with the imaginary part of the Green dyadic evaluated at the position of the source [43]:

$$\Gamma = \frac{4\omega^2}{\pi c^2 \hbar \varepsilon_0} \left[\vec{\mu} \cdot Im \left\{ \overleftrightarrow{G}(r_0, r_0) \right\} \cdot \vec{\mu} \right], \tag{5}$$

where ω is the frequency of emission of the source, ε_0 is the vacuum dielectric constant, c the speed of light in vacuum, $\hbar$ the reduced Planck constant, and μ the dipole moment of the source. Figure 1 shows a layout of a section of the waveguide used for our model. The waveguide (infinite in the z-axis) has a rectangular section filled with a linear homogeneous medium with refractive index n_1. The surrounding environment has a refractive index $n_2 = 1$.

The calculation of the Green's Dyadic is based on the development of a 3D transform theory applied to the unbounded Helmholtz equation. Details of the calculation and the explicit

Optics EXPRESS

dependence with the waveguide width and the position/orientation of the source (for each contributing guided mode) can be found in the Supplement 1. Using the Green's dyadic we can obtain the Purcell enhancement as a function of the waveguide width for a point dipolar source that can be oriented parallel to the x-axis (s) or to the y-axis (p). The source is placed initially at the center of the waveguide cross-section ($x_0 = 0$, $y_0 = 0$). Initially, the waveguide thickness is arbitrarily fixed at $b = 200$ nm and we will change the width (a) and the refractive index of the waveguide (n_1) using $n_1 = 1.44$, 2 and 3.4 corresponding to SiO_2, SiN and Si respectively. This will provide some initial hints on how the system actually behaves.

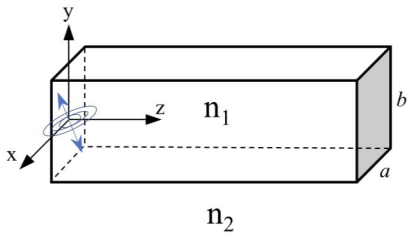

Fig. 1. Layout of the homogeneous infinite waveguide used for the analytical model.

Figure 2 shows the value of the Purcell enhancement, Γ/Γ_0, as a function of the normalized waveguide width, a/λ, for the mentioned values of n_1 (1.44, 2, 3.4). Solid lines show the calculation of Γ/Γ_0 using Eq. (5) and open dots show the values obtained through FDTD simulations. Details of the FDTD simulations can be found in the Supplement 1. Figure 2(a) shows the Purcell enhancement for the s-source. In general, it almost vanishes before the width reaches the cut-off of the TE_{10} mode, which happens for $a/\lambda = 0.13$, 0.1 and 0.05 for $n_1 = 3.4$, 2 and 1.44, respectively. Since the cut-off increases with n_1, the vanishing threshold also increases with n_1. After the cut-off, for increasing a/λ, The Purcell enhancement increases as the propagation constant decreases (with $1/a$) and the mode gets more confined. The maximum values for Γ/Γ_0 are 0.83, 1 and 1 when $a/\lambda = 0.23$, 0.42 and 0.64 respectively and the light confinement is maximum. If the waveguide becomes wider the modes spread out with lower intensity at the position of the source producing a decrease in Γ/Γ_0 that scales with $1/a$, until the cut-off with the second order mode is reached at a/λ=0.43, 0.8 and 1.2 for the same values of n_1. At this point, the same mechanism takes place showing the second maxima and second decay. The process is repeated for each contributing mode. We note that there is no contribution from the lowest TM_{00} mode because the components of the Green dyadic vanish at the position of the source for this orientation. This is expected since the x-components of the fundamental modes are antisymmetric with respect to the source when it is placed at the center. For the p-source [Fig. 2(a)] the situation is somewhat opposite and the components do not vanish at the position of the source for the lowest order TM_{00}. Since $b = 200$ nm, in the case of $n_1 = 2$ and $n_1 = 1.44$ the cut-off condition is already reached at $a/\lambda = 0$. For $n_1 = 3.4$ the cut-off is reached at $a/\lambda = 0.05$. The Purcell enhancement for the s-source shows maximum values of $\Gamma/\Gamma_0 = 1.2$, 0.51 and 0.6 when $a/\lambda = 0.13$, 0.27 and 1 for the same values of n_1 than before. For both s and p orientations the Purcell enhancement decays asymptotically with the width, although in a different trend due to the different (m, n) values for each contributing mode. The maxima located at a/λ=0 are accidentally generated by the model due to the unphysical divergence of the Green function at the origin. The maximum values of Γ/Γ_0 for the s-source are about 40% higher than for the p-source with $n_1 = 2$ and $n_1 = 1.44$. The reason is the transverse electric field component of the TE_{10}, which is higher than the TM_{00} at the position of the source ($x_0 = 0$, $y_0 = 0$) [44]. Nevertheless, for $n_1 = 3.4$ the maximum Γ/Γ_0 is about 40% higher for the p-source. This happens because when $n_1 = 2$ and $n_1 = 1.44$ the TE_{10} mode is well confined for b=200 nm, but when $n_1 = 3.4$ the TE_{10}

Optics EXPRESS

mode is not optimally confined and the source has a better overlap with the TM_{00}. Therefore, high modal confinement and good spatial overlapping to waveguide modes are key ingredients for Purcell enhancement, as one could intuitively expect. The indistinguishability should show its maximum value when the Purcell enhancement is maximum, according to Eq. (3). We note that a deviation in the optimal width of about 20 nm can decrease the Purcell enhancement, and therefore the indistinguishability, about 10%.

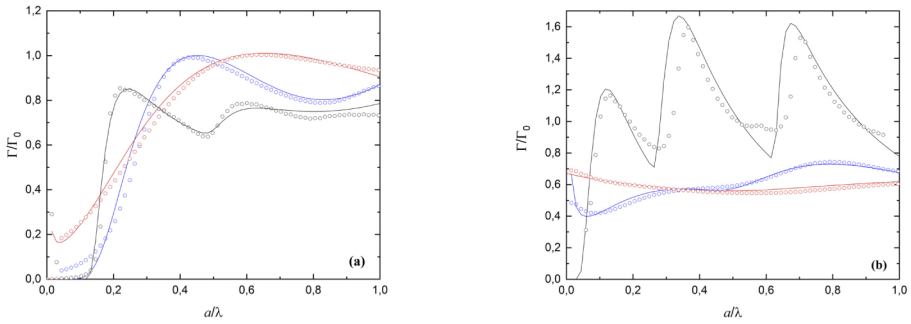

Fig. 2. Purcell enhancement of the radiative decay rate as a function of the wavelength-normalized waveguide width obtained from analytical calculations (lines) and FDTD simulations (open dots). $n_1 = 3.4$ (black), $n_1 = 2$ (blue), $n_1 = 1.44$ (red). (a) Source orientation parallel to x-axis (s); (b) Parallel to y-axis (p).

Since the position of the emitter is very relevant, we explore now its effect keeping fixed the waveguide widths in a/λ=0.23, 0.42 and 0.64 (respectively to the n_1 values as before) and for the s orientation. We change the position of the source along the x-axis, from the center of the waveguide (x_0/a=0) to far away from the edge ($x_0/a>\pm1$).

First we focus on the region inside the waveguide core ($x_0/a<\pm1$). Figure 3(a) shows the Purcell enhancement depending on the position of the s-source. As the s-source is separated from the center the overlapping to symmetric modes decreases and the enhancement decreases. The maximum enhancement happens at the center of the waveguide. A deviation from that optimal position of about $x_0/a=\pm0.5$ leads to a decrease of the Purcell enhancement of about 20%. The opposite behavior is obtained for a p-source [Fig. 3(b)]. In this case the minimum overlapping is obtained at the center of the waveguide and the maximum enhancement is for about $x_0/a=\pm0.75$, where the overlap with the antisymmetric modes is maximum. FDTD simulations provide a maximum value for the enhancement of 1.42 matching the analytical calculations within an error of 0.2% for the Purcell enhancement and 0.3% for x_0.

The variation of the *coupling efficiency* with the position of the source inside the waveguide follows a similar trend than the Purcell enhancement. Details of coupling definition and its calculation can be found in the Supplement 1. Figure 4 shows the coupling efficiency depending on the position of the source for both s and p orientations. At the center of the waveguide, the s-source achieves a maximum coupling of $P_c/P_0 = 0.88$, 0.6 and 0.25 for $n_1 = 3.4$, 2 and 1.44 respectively, where P_c is the emitted power coupled to guided modes. As expected, the coupling decreases with decreasing n_1. When the s-source is separated from the center, the coupling to symmetric modes decreases. Again, the opposite behavior is obtained for the p-source, which shows minimum coupling at the center of the waveguide. Some discrepancies between analytic and FDTD results arise from the discretization of space in the FDTD simulations. Also, the slight asymmetries shown in the x_0/a dependence in Fig. 4(b) are due to small misalignments between the simulation cells and the dielectric waveguide.

Since there are recent experimental works that use heterogeneous integration of SPS and waveguides [45,46] it is worth to explore the dependence of the enhancement with the position of

Optics EXPRESS

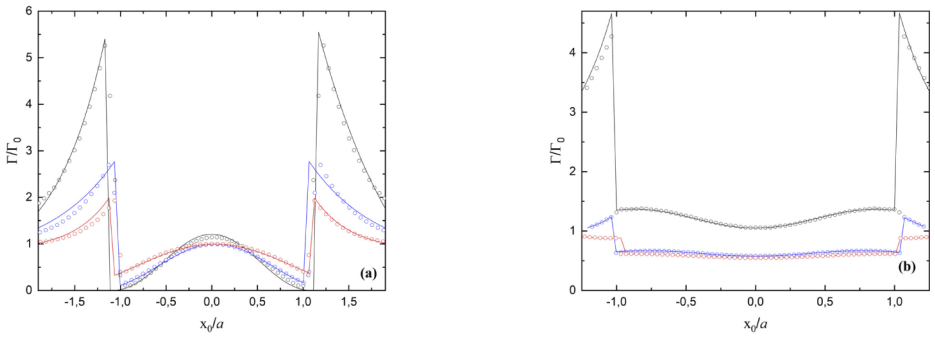

Fig. 3. Enhancement of the radiative decay rate as a function of the position of the point source (normalized with respect to the waveguide width, (a) obtained from the analytical model (lines) and from FDTD simulations (open dots). The origin in the x-axis corresponds to the center of the waveguide and the edges to x_0/a=±1. $n_1 = 3.4$ (black), $n_1 = 2$ (blue), $n_1 = 1.44$ (red). (a) s-source (b); p-source.

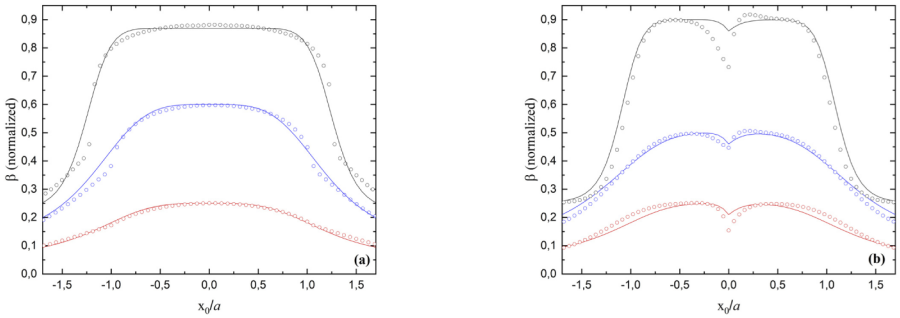

Fig. 4. Coupling efficiency versus normalized position of the source with respect to waveguide width a. The origin in the x-axis corresponds to the center of the waveguide. The edges of the waveguide correspond to x_0/a=±1. Figure shows results from analytical model (lines) and from FDTD simulations (open dots). $n_1 = 3.4$ (black), $n_1 = 2$ (blue), $n_1 = 1.44$ (red). (a) s-source; (b) p-source.

the source in the region outside the waveguide but close to its edge (x_0/a>±1). Due to the index contrast between air and waveguide the electric field shows a strong discontinuity at the interface with an amount comparable to the square of the index ratio at the interface [47]. This effect can lead to a dramatic alteration of the mode profile in the vicinity of the edge that drastically increments the Purcell enhancement. This effect has been used, for example, to achieve ultrasmall cavity mode volumes of the order of $7 \times 10^{-5}\lambda^3$ that enable ultra-strong Kerr nonlinearities at the single-photon level [48]. When the source is placed at the edge the enhancement is Γ/Γ_0=4.2, 2.6 and 1.9 for the s-source, and Γ/Γ_0=4.6, 1.2 and 0.87 for the p-source. The cost of the increase in the Purcell enhancement is a decrease in the coupling efficiency, which for the position at the edge is about $P_c/P_0 = 0.5$, 0.37 and 0.15 for the s-source and about $P_c/P_0 = 0.5$, 0.3 and 0.12 for the p-source. Details about this calculation can be seen in the Supplement 1. At the points x_0/a=±1 (i.e., the edges of the waveguide) the mode field shows its highest contrast according to $E_{\text{clad}} = (n_1/n_2)^2 E_{\text{core}}$ where E_{core} is the field inside the waveguide and E_{clad} is the field outside the waveguide. For that reason, the maximum value of the Purcell enhancement lies in the edges of the waveguide, especially for high n_1. Since the Purcell enhancement is strictly dependent on the field value at the position of the source, its maximum value is achieved at the edge of the waveguide. On the other hand, the coupling is proportional to the guided-mode field value

Optics EXPRESS

divided by the non-guided modes field value. Despite the guided-mode field value is maximum at the edge, the value of non-guided modes is also maximum at the edge. In consequence, the coupling at the edge is weaker than in the center of the core (where the coupling to non-guided modes is smaller).

Now that we have a better understanding of the physical meaning of the model we can explore simultaneously both degrees of freedom (i.e., a and b) in order to find the optimal configurations in terms of the figures of merit. The source is placed initially at the center of the waveguide cross-section ($x_0 = 0$, $y_0 = 0$) in horizontal orientation (i.e., parallel to x-axis) but this time both a and b are varied from 0 to 0.7 λ. The results are obtained for four different values of the refractive index of the waveguide $n_1 = 1.44$, 2, 3.4, and 4.

Figure 5 shows the value of Γ/Γ_0 as a function of the normalized waveguide width, a/λ, and normalized thickness, b/λ, calculated for the four different refractive indexes. The blue areas in the plots correspond to values of a and b below the first cut-off. The subsequent maxima and minima correspond to the activation of the TE_{mn} and TM_{mn} modes. For low refractive indexes (i.e., $n_1 = 1.44$, 2) the two first modes appear. As the refractive index increases the source starts to overlap effectively with the rest of higher order modes. The absolute maxima of Γ/Γ_0 increases with the refractive index, since the area of the spatial distribution of the modes decreases with n_1, so the field intensity gets higher at the position of the source. We obtain maximum values of Γ/Γ_0=1, 1.1, 1.6 and 1.9 for $n_1 = 1.44$, 2, 3.4 and 4, respectively. Due to the symmetry of the system the plots for the vertical source show the same rotated 90 degrees (see Supplement 1).

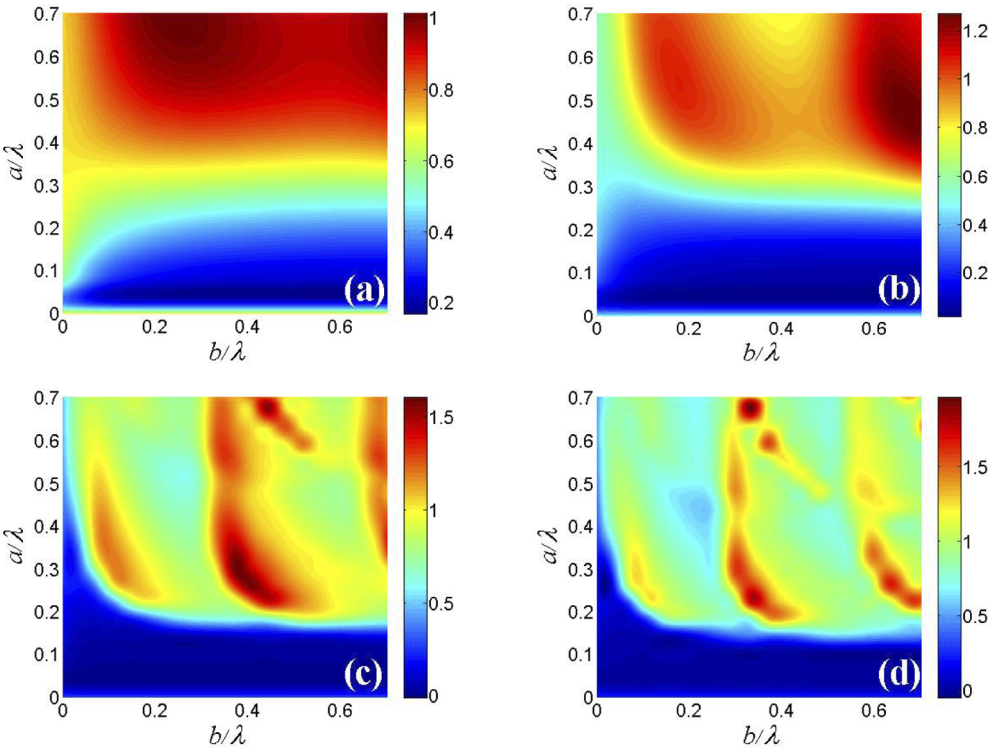

Fig. 5. Purcell enhancement as a function of the normalized width, a/λ, and thickness, b/λ, when the s-source is placed at the center of the waveguide calculated with the analytical model. (a) $n_1 = 1.44$; (b) $n_1 = 2$; (c) $n_1 = 3.4$; (d) $n_1 = 4$.

Next, we place the source outside the waveguide, 10 nm away from the edge and oriented horizontally (i.e., parallel to x-axis). Figure 6 shows the value of Γ/Γ_0 as a function of the

Optics EXPRESS

normalized waveguide width, a/λ, and normalized thickness, b/λ, for different n_1. As we saw before, the field discontinuity generates a dramatic enhancement when the source is placed near the evanescent region of the mode. We observe that in all of the cases the maxima are located in the bottom left region, where both a and b have reached the cut-off but the first mode has not reached the maximum confinement. For that geometry, the mode is not optimally confined inside the core and the field gets accumulated at the edges of the waveguide so the overlap is more efficient. We obtain maximum values of $\Gamma/\Gamma_0 = 2,\ 3.5,\ 8$ and 10 for $n_1 = 1.44$, 2, 3.4 and 4 respectively. At this time the orientation of the source matters, since we can arrange two different configurations: (a) Parallel to the larger side of the waveguide (i.e., parallel to the x-axis if the source is placed on top of the core, or parallel to the y-axis if the source is placed on one side of the core); (b) Perpendicular to the larger side of the waveguide (i.e., parallel to the y-axis if the source is placed on top of the core, or parallel to the x-axis if the source is placed on one side of the core). The plots in Fig. 6 correspond to the second case. When the source is parallel we obtain lower values for the maximum enhancements: $\Gamma/\Gamma_0 = 0.9,\ 1.5,\ 6.8$ and 7.1 for the different values of n_1. For emitters with orientations other than s or p one should decompose the projection of the orientation on the x-axis and the y-axis and treat the emitter as two separated emitters with corresponding s and p contributions. The total enhancement is given by the addition of those two contributions.

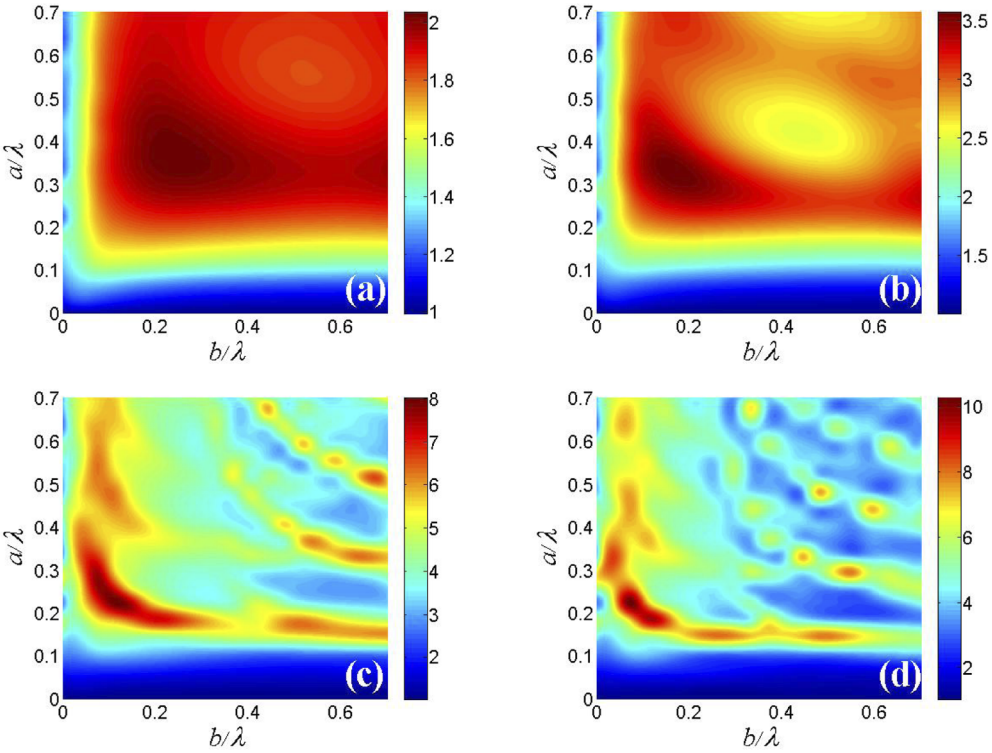

Fig. 6. Purcell enhancement as a function of a/λ and b/λ when the s-source is placed outside the core calculated with the analytical model. (a) $n_1 = 1.44$, (b) $n_1 = 2$, (c) $n_1 = 3.4$, (d) $n_1 = 4$.

The maximum enhancements obtained for the source at the edge can be used in Eq. (3) to obtain the maximum values for the indistinguishability. Figure 7 shows I for an s-emitter placed at the edge of the waveguide versus the intrinsic emitter normalized dephasing ratio, Γ^*/Γ_0. Results for the p-source show an analogous behavior. From Fig. 7 we see that for *low*

Optics EXPRESS

dissipative emitters with $\Gamma^*/\Gamma_0 \sim 1$ (like weakly confined GaAs dots of Ref. [13]) the expected indistinguishability can reach a value up to 0.8 when $n_1 = 4$, which makes an enhancement of I of about 30% with respect to the same dots without coupling to a waveguide. For InAs quantum dots with $\Gamma^*/\Gamma_0 = 2.6$ [36,37] we obtain $I \approx 0.6$, an enhancement of 40%. As the pure dephasing rate increases the indistinguishability decays asymptotically reaching 0.2 when $\Gamma^*/\Gamma_0 = 50$. Therefore for strong dissipative systems with $\Gamma^*/\Gamma_0 > 50$ (like quantum emitters in 2D materials) the effect of the waveguide in the indistinguishability is very small. For emitters with lower dephasing ratio, $\Gamma^*/\Gamma_0 < 1$, and high intrinsic indistinguishability ($I >> 0.5$) the effect of the waveguide becomes again negligible since $I \rightarrow 1$ when $\Gamma^*/\Gamma_0 \rightarrow 0$. As n_1 increases the maximum Γ^*/Γ_0 for $I >> 0.5$ also increases reaching values up to 12 for $n_1 = 4$.

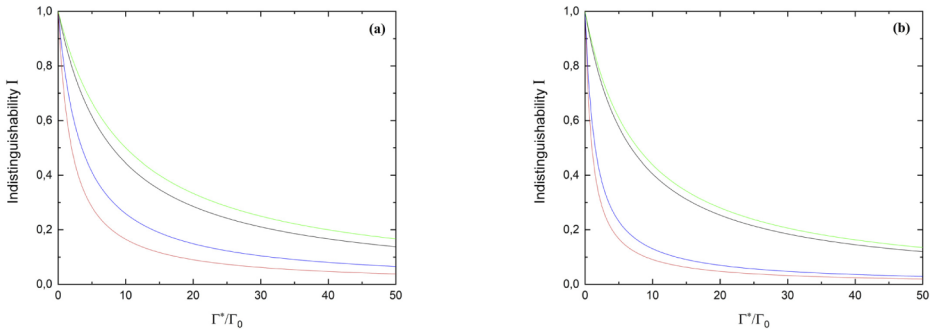

Fig. 7. Indistinguishability of an s-source quantum emitter placed at the edge of the waveguide versus its $\frac{\Gamma^*}{\Gamma_0}$ value. Green- $n_1 = 4$, Black– $n_1 = 3.4$, Blue- $n_1 = 2$, Red- $n_1 = 1.44$. (a) Perpendicular-source. (b) Parallel-source.

Despite a SPS can achieve much stronger Purcell enhancements inside optical cavities [49], it is often required small mode volumes or high quality factors, or both. Small mode volumes difficult the deposition of the emitter at the field maxima [50], and on the other hand, high quality factors reduce the extraction efficiency [34]. In the case of waveguide integration, deposition at the field maxima (i.e., edge of the waveguide) becomes trivial, and as it has been shown, high extraction efficiency can be achieved. However, our results also reveal that for strong dissipative SPS integrated in a waveguide the indistinguishability does not reach the standard requirements for quantum information applications. For those cases the use of an optical cavity is mandatory.

From a practical perspective, the heterogeneous integration of the emitter with a waveguide may be performed by placing the emitter inside a material with non-unity refractive index (i.e., $n_2 \neq 1$) [45], it is worth to explore how the Purcell enhancement is affected by different index contrasts. As we mentioned above, the field discontinuity at the edge of the waveguide is proportional to $(n_1/n_2)^2$, so we can expect a significant reduction of the enhancement depending on n_2.

Figure 8(a) shows the dependence of the Purcell enhancement with n_2 for an s-source placed at the edge of the waveguide with optimal (a,b) geometry. Since the Purcell enhancement in the edge depends on the index contrast n_1/n_2, it decreases asymptotically with n_2. In the limit where $n_2 \sim 1$ the Purcell value approaches to that shown in Fig. 6, and when $n_2 \sim n_1$ we obtain the emitter decay rate corresponding to a homogeneous material (i.e., $P_f = 1$). For cladding materials like SiO_2 ($n_2 = 1.44$) the Purcell enhancement is reduced about 50% with respect to the value with $n_2 = 1$. On the other hand, Fig. 8(b) shows the reduction in the indistinguishability due to this lower Purcell enhancement for an emitter with $\Gamma^*/\Gamma_0 = 10$. Similarly to what happened to the Purcell enhancement, when $n_2 \sim 1$ the indistinguishability approaches to that shown in Fig. 7, and when $n_2 \sim n_1$ we obtain the value corresponding to the specific Γ^*/Γ_0 ratio in a homogeneous material (i.e., $I = 0.1$). Again, for $n_2 = n_{SiO2}$ the indistinguishability is reduced about 15% with respect to $n_2 \sim 1$. Regarding the optimization sweep for finding the optimal waveguide height and

Optics EXPRESS

width for the case of n_2 in the range (1–1.6) the results are almost equivalent to that shown in Fig. 6 (case of $n_1 = 1.44$). Therefore Fig. 6 can be used as a guide for waveguide design when n_2 is inside that range.

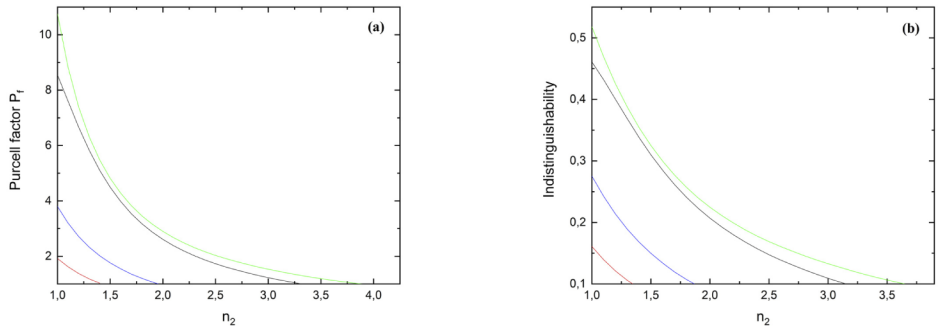

Fig. 8. (a) Purcell enhancement of an *s*-source at the edge of the waveguide as a function of n_2. (b) Indistinguishability of an *s*-source at the edge of the waveguide as a function of n_2.

It is important to highlight that the positions for maximum indistinguishability differ from those of maximum coupling efficiency. Indistinguishability depends strongly on Purcell enhancement, which for the case of a waveguide achieves its maximum value at the edge, where the field is strongest. On the other side, the coupling efficiency on the edge is not as high as in the center, but still may have a value useful for some experiments or even some applications An interesting figure of merit for the geometrical optimization of the waveguide is the $I \cdot \beta$ product (with β the coupling efficiency) that can be explored as a function of a and b. In the same way we did for the optimization of the Purcell enhancement, a and b change from 0 to 0.7 λ, and the emitter is placed at the edge of the waveguide. We set $n_2 = 1.44$ this time and we vary $n_1 = 2$, 3.4, 4 and 4.4. For the estimation of the indistinguishability we set Γ^*/Γ_0=10 as before.

Figure 9 shows the $I\ \beta$ value as a function of the normalized waveguide width, a/λ, and normalized thickness, b/λ, calculated for $n_1 = 2$, 3.4, 4 and 4.4. As expected, for the four refractive indexes the highest $I\ \beta$ happens for the geometry that maximizes the Purcell enhancement. Maximum $I\ \beta = 0.35$ is found for the highest waveguide index ($n_1 = 4.5$) and minimum $I\ \beta = 0.15$ for $n_1 = 2$. Also, in the four cases the $I\ \beta$ product is significantly higher than the obtained when the source is at the center of the waveguide (0.06 for $n_1 = 2$, 0.09 $n_1 = 3.4$, and 0.13 for $n_1 = 4$).

2.3. Analytic model for spectral diffusion

We have explored so far the effect of pure dephasing in the indistinguishability. In addition, the effect of spectral diffusion needs to be treated separately. Whereas the dynamics of pure dephasing evolve at shorter time scales than the emitter decay rate Γ_0, spectral diffusion is related to processes with significantly larger time scales [51] so it is characterized by a statistical average over the different center frequencies associated with the emitter [52]. In this context, the spectral broadening of the emission is given by $\Gamma_2 = \Gamma_0 + \Gamma'$, where Γ' represents the FWHM of the distribution associated with spectral diffusion. The indistinguishability reads $I = \Gamma_0/\Gamma_2$ [51]. Being $\Delta\omega$ the intrinsic width of each center frequency, and $\Delta\delta$ the extrinsic width due to the entanglement with the extrinsic environment, for a Lorentzian distribution the ratio $\theta = \Delta\delta/\Delta\omega$ is equal to $2\Gamma'/\Gamma_0$ [52]. The indistinguishability can be written in terms of θ as:

$$I = \frac{\Gamma/\Gamma_0}{\Gamma/\Gamma_0 + \frac{\theta}{2}}, \tag{6}$$

Optics EXPRESS

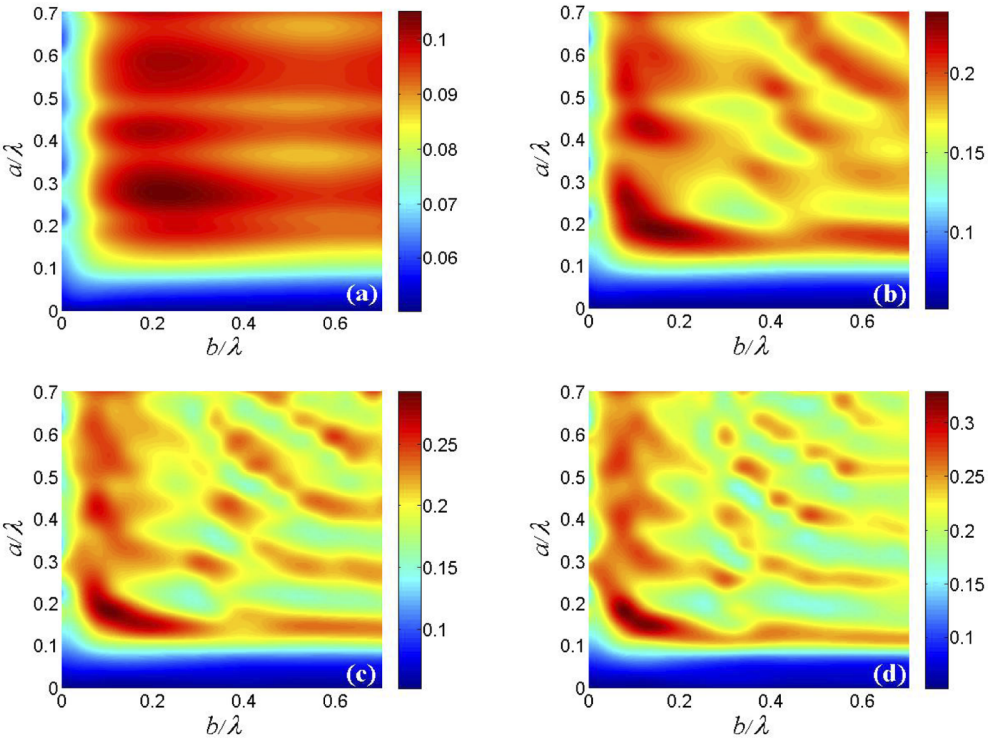

Fig. 9. I β value as a function of the normalized width, a/λ, and thickness, b/λ, when the s-source is placed at the edge of the waveguide with $n_2 = 1.44$ calculated with the analytical model. (a) $n_1 = 2$, (b) $n_1 = 3.4$, (c) $n_1 = 4$, (d) $n_1 = 4.5$.

with Γ the enhanced decay rate due to Purcell effect. As we did in the previous section, we can use the maximum enhancements obtained for the source at the edge in Eq. (6) to obtain the maximum values for the indistinguishability.

Figure 10 shows I for s- and p-emitters placed at the edge of the waveguide versus the normalized ratio θ. From Fig. 1 we see that for emitters with with $\theta \sim 1$ [13] the expected indistinguishability is above 0.9 for the four refractive indexes. As the extrinsic width of the

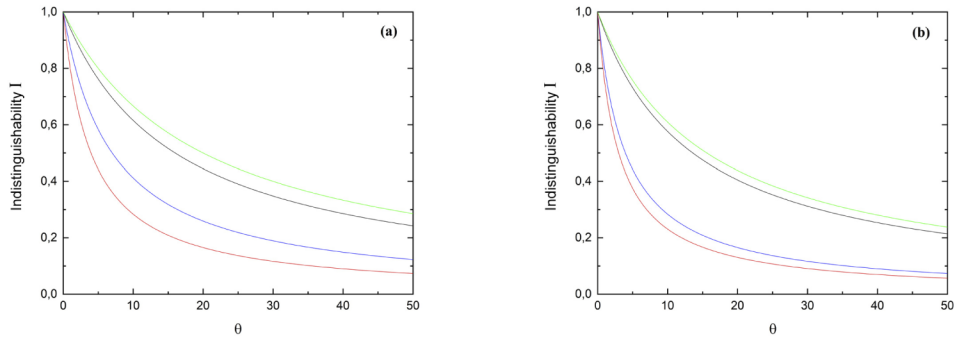

Fig. 10. Indistinguishability of an s-source quantum emitter placed at the edge of the waveguide versus its $\theta <$ value. Green- $n_1 = 4$, Black– $n_1 = 3.4$, Blue- $n_1 = 2$, Red- $n_1 = 1.44$. (a) Parallel-source. (b) Perpendicular-source.

Optics EXPRESS

emitter increases respect to the intrinsic width the indistinguishability decays asymptotically reaching 0.3 when $\theta = 50$ for $n_1 = 4$ and $\theta = 10$ for $n_1 = 1.44$. Therefore, for emitters with extrinsic width much larger than intrinsic width the effect of the waveguide in the indistinguishability is negligible. As n_1 increases the maximum θ for $I >> 0.5$ also increases reaching values up to 21 for $n_1 = 4$. We can say that in general we observe a similar behavior to pure dephasing although with a slower asymptotic decay of I.

3. Conclusions

We have calculated the indistinguishability of a point-source quantum emitter coupled to a waveguide because its technological implications in future quantum photonic integrated circuits. The emitter has arbitrary orientation and location with respect to the waveguide. We have obtained the results for different index of refraction of the waveguide (SiO_2, Si_3N_4, Si, and other high index materials like WeS_2 or WO_3). The analytical model used permits a fast computing of the indistinguishability from a set of simple expressions derived from the same solution of the dyadic Helmholtz equation. The model has been numerically evaluated through 3D-FDTD simulations with excellent agreement. Maximum indistinguishability for an optimal waveguide width is found for a source placed outside the core, at the edge of the waveguide, in contrast to maximum coupling efficiency position at the center of the waveguide. For strong dissipative emitters with $\Gamma^*/\Gamma_0 > 50$ (like transition metal dichalcogenides) the effects of the waveguide in the indistinguishability are negligible but for low dissipative emitters with $\Gamma^*/\Gamma_0 \approx 1$ (like GaAs quantum dots) the indistinguishability can be enhanced up to a 30% and reach values around $I \approx 0.8$ when dots are coupled to a waveguide. We hope this work can help for an optimized design of PIC waveguides in quantum photonic circuits.

Funding. Horizon 2020 Framework Programme (820423).

Acknowledgments. We gratefully acknowledge financial support from the European Union's Horizon 2020 research and innovation program under grant agreement No. 820423 (S2QUIP).

Disclosures. The authors declare that there are no conflicts of interest related to this article.

Data availability. All the data generated and analyzed in this work are available upon request.

Supplemental document. See Supplement 1 for supporting content.

References

1. A. Aspuru-Guzik and P. Walther, "Photonic quantum simulators," Nat. Phys. **8**, 285–291 (2012).
2. D. Fattal, E. Diamanti, K. Inoue, and Y. Yamamoto, "Quantum teleportation with a quantum dot single photon source," Phys. Rev. Lett. **92**, 037904 (2004).
3. H. Kimble, "The quantum internet," Nature (London) **453**, 1023–1030 (2008).
4. M. Eisaman, J. Fan, A. Migdall, and S. Polyakov, "Invited Review Article: Single-photon sources and detectors," Rev. Sci. Instrum. **82**, 071101 (2011).
5. C. Santori, D. Fattal, J. Vučković, G. S. Solomon, and Y. Yamamoto, "Indistinguishable photons from a single-photon device," Nature **419**, 594–597 (2002).
6. Y. Chen, J. Zhang, M. Zopf, K. Jung, Y. Zhang, R. Keil, and O. G. Schmidt, "Wavelength-tunable entangled photons from silicon-integrated III–V quantum dots," Nat. Commun. **7**, 1–7 (2016).
7. S. Khasminskaya, F. Pyatkov, K. Słowik, S. Ferrari, O. Kahl, V. Kovalyuk, P. Rath, A. Vetter, F. Hennrich, M. M. Kappe, G Gol'tsman, A. Korneev, C. Rockstuhl, R. Krupke, and W. H. P. Pernice, "Fully integrated quantum photonic circuit with an electrically driven light source," Nat. Photonics **10**, 727–732 (2016).
8. S. L. Mouradian, T. Schröder, C. B. Poitras, L. Li, J. Goldstein, E. H. Chen, and M. Lipson, "Scalable integration of long-lived quantum memories into a photonic circuit," Phys. Rev. X **5**, 031009 (2015).
9. A. Sipahigil, R. E. Evans, D. D. Sukachev, M. J. Burek, J. Borregaard, M. K. Bhaskar, and R. M. Camacho, "An integrated diamond nanophotonics platform for quantum-optical networks," Science **354**, 847–850 (2016).
10. F. Peyskens, C. Chakraborty, M. Muneeb, D. Van Thourhout, and D. Englund, "Integration of single photon emitters in 2D layered materials with a silicon nitride photonic chip," Nat. Commun. **10**, 4435–4437 (2019).
11. A. Kiraz, M. Ehrl, T. Hellerer, ÖE Müstecaplıoğlu, C. Bräuchle, and A. Zumbusch, "Indistinguishable photons from a single molecule," Phys. Rev. Lett. **94**, 223602 (2005).
12. J. M. Gérard, B. Sermage, B. Gayral, B. Legrand, E. Costard, and V. Thierry-Mieg, "Enhanced spontaneous emission by quantum boxes in a monolithic optical microcavity," Phys. Rev. Lett. **81**, 1110–1113 (1998).

Optics EXPRESS

13. D. Gammon, E. S. Snow, B. V. Shanabrook, D. S. Katzer, and D. Park, "Homogeneous linewidths in the optical spectrum of a single gallium arsenide quantum," Science **273**, 87–90 (1996).
14. I. Aharonovich, D. Englund, and M. Toth, "Solid-state single-photon emitters," Nat. Photonics **10**, 631–641 (2016).
15. Ł. Dusanowski, D. Köck, E. Shin, S. H. Kwon, C. Schneider, and S. Höfling, "Purcell enhanced and indistinguishable single-photon generation from quantum dots coupled to on-chip integrated ring resonators," Nat. Photonics **20**, 6357–6363 (2020).
16. X. Qiang, X. Zhou, J. Wang, C. M. Wilkes, T. Loke, S. O'Gara, and J. B. Wang, "Large-scale silicon quantum photonics implementing arbitrary two-qubit processing," Nat. Photonics **12**, 534–539 (2018).
17. J. Wang, F. Sciarrino, A. Laing, and M. G Thompson, (2019). "Integrated photonic quantum technologies," *Nat. Photonics* 1–12.
18. S. Slussarenko and G. J. Pryde, "Photonic quantum information processing: A concise review," Appl. Phys. Rev. **6**, 041303 (2019).
19. C. T. Chen, J. Pedrini, E. A. Gaulding, C. Kastl, G. Calafiore, S. Dhuey, and A. M. Schwartzberg, "Very high refractive index transition metal dichalcogenide photonic conformal coatings by conversion of ALD metal oxides," Sci. Rep. **9**, 1–9 (2019).
20. Y. He, S. He, J. Gao, and X. Yang, "Nanoscale metamaterial optical waveguides with ultrahigh refractive indices," J. Opt. Soc. Am. B **29**, 2559–2566 (2012).
21. W. Huang, A. B. Yakovlev, A. A. Kishk, and A. W. Glisson, (2006). *Dyadic Greens Function of the Hard Surface Rectangular Waveguide Verified Numerically by a Realistic Model*. In 2006 IEEE Antennas and Propagation Society International Symposium (pp. 2249–2252). IEEE.
22. W. Huang, A. B. Yakovlev, A. A. Kishk, A. W. Glisson, and I. A. Eshrah, "Green's function analysis of an ideal hard surface rectangular waveguide," Radio Sci. **40**, 1–12 (2005).
23. X. Zhang, C. Xu, and W Song, "Calculating higher order mode characteristics of heteromorphic waveguide by operator theory," in 2000 Asia-Pacific Microwave Conference. Proceedings (Cat. No. 00TH8522) (2000). pp. 970–974
24. P. M. Słobodzian, "On the dyadic Green's function in the source region embedded in waveguides or cavities filled with a stratified medium," Microwave and Optical Technology Letters **35**, 93–97 (2002).
25. V. A. Klymko, A. B. Yakovlev, I. A. Eshrah, A. A. Kishk, and A. W. Glisson, "Dyadic Green's function of an ideal hard surface circular waveguide with application to excitation and scattering problems," Radio Sci. **40**, 1–15 (2005).
26. S. Liu, L. W. Li, M. S. Leong, and T. S. Yeo, "Rectangular conducting waveguide filled with uniaxial anisotropic media: A modal analysis and dyadic Green's function," Prog. Electromagn. Res. **25**, 111–129 (2000).
27. S. R. J. Brueck, "Radiation from a dipole embedded in a dielectric slab," IEEE J. Sel. Top. Quantum Electron. **6**, 899–910 (2000).
28. C. Creatore and L. C. Andreani, "Quantum theory of spontaneous emission in multilayer dielectric structures," Phys. Rev. A **78**, 063825 (2008).
29. F. Santosa and R. Magnanini, "Wave propagation in a 2-D optical waveguide," SIAM J. Appl. Math. **61**, 1237–1252 (2001).
30. O. Alexandrov and G. Ciraolo, "Wave propagation in a 3-D optical waveguide," Math. Models Methods Appl. Sci. **14**, 819–852 (2004).
31. G. Ciraolo, F. Gargano, and V. Sciacca, "A computational method for the Helmholtz equation in unbounded domains based on the minimization of an integral functional," J. Comput. Phys. **246**, 78–95 (2013).
32. O. Alexandrov, "The far-field expansion of the Green's function in a 3-D optical waveguide," Asymptot. Anal. **52**, 157–171 (2007).
33. J. Bylander, I. Robert-Philip, and I. Abram, "Interference and correlation of two independent photons," Eur. Phys. J. D, **22**, 295–301 (2003).
34. T. Grange, G. Hornecker, D. Hunger, J. P. Poizat, J. M. Gérard, P. Senellart, and A. Auffèves, "Cavity-funneled generation of indistinguishable single photons from strongly dissipative quantum emitters," Phys. Rev. Lett. **114**, 193601 (2015).
35. E. Schöll, L. Hanschke, L. Schweickert, K. D. Zeuner, M. Reindl, S. F. Covre da Silva, and A. Rastelli, "Resonance fluorescence of gaas quantum dots with near-unity photon indistinguishability," Nano Lett. **19**, 2404–2410 (2019).
36. J. M. Gérard, O. Cabrol, and B. Sermage, *Appl. Phys. Lett.* 68, 3123 (1996).
37. P. Borri, W. Langbein, S. Schneider, U. Woggen, R. L. Sellin, D. Ouyang, and D. Bimberg, "Ultralong dephasing time in InGaAs quantum dots," Phys. Rev. Lett. **87**, 157401 (2001).
38. J. Klein, M. Lorke, M. Florian, F. Sigger, L. Sigl, S. Rey, and P. Zimmermann, "Site-selectively generated photon emitters in monolayer MoS 2 via local helium ion irradiation," Nat. Commun. **10**, 1–8 (2019).
39. C. Chakraborty, N. Vamivakas, and D. Englund, "Advances in quantum light emission from 2D materials," Nanophotonics **8**, 2017–2032 (2019).
40. L. N. Tripathi, O. Iff, S. Betzold, Ł. Dusanowski, M. Emmerling, K. Moon, and C. Schneider, "Spontaneous emission enhancement in strain-induced WSe2 monolayer-based quantum light sources on metallic surfaces," ACS Photonics **5**, 1919–1926 (2018).
41. R. Chaudhary, V. Raghunathan, and K. Majumdar, "Origin of selective enhancement of sharp defect emission lines in monolayer WSe2 on rough metal substrate," J. Appl. Phys. **127**, 073105 (2020).
42. S. Wein, N. Lauk, R. Ghobadi, and C. Simon, "Feasibility of efficient room-temperature solid-state sources of indistinguishable single photons using ultrasmall mode volume cavities," Phys. Rev. B **97**, 205418 (2018).

Optics EXPRESS

43. L. Novotny and B. Hecht, "Principles of nano-optics," (Cambridge University Press, 2012), pp 58.
44. S. L. Chuang, "Physics of Optoelectronic Devices," in Wiley Series in Pure and Applied Optics (Wiley, 1995), 22.
45. P. Lombardi, A. P. Ovvyan, S. Pazzagli, G. Mazzamuto, G. Kewes, O. Neitzke, and C. Toninelli, "Photostable molecules on chip: integrated sources of nonclassical light," ACS Photonics **5**(1), 126–132 (2018).
46. C. Errando-Herranz, E. Schöll, M. Laini, S. Gyger, A. W. Elshaari, A. Branny, and C. Bonato (2020). On-chip single photon emission from a waveguide-coupled two-dimensional semiconductor. arXiv preprint arXiv:2002.07657.
47. S. Majumder and R. Chakraborty, "Semianalytical method to study silicon slot waveguides for optical sensing application," Opt. Eng. **52**(10), 107102 (2013).
48. H. Choi, M. Heuck, and D. Englund, "Self-similar nanocavity design with ultrasmall mode volume for single-photon nonlinearities," Phys. Rev. Lett. **118**(22), 223605 (2017).
49. F. Pisanello, A. Qualtieri, T. Stomeo, L. Martiradonna, R. Cingolani, A. Bramati, and M. De Vittorio, "High-Purcell-factor dipolelike modes at visible wavelengths in H1 photonic crystal cavity," Opt. Lett. **35**(10), 1509–1511 (2010).
50. J. T. Hugall, A. Singh, and N. F. van Hulst, "Plasmonic cavity coupling," Acs Photonics **5**(1), 43–53 (2018).
51. H. Choi, D. Zhu, Y. Yoon, and D. Englund, "Cascaded cavities boost the indistinguishability of imperfect quantum emitters," Phys. Rev. Lett. **122**(18), 183602 (2019).
52. F. W. Sun and C. W. Wong, "Indistinguishability of independent single photons," Phys. Rev. A: At., Mol., Opt. Phys. **79**(1), 013824 (2009).